Organic Electronics 82 (2020) 105714

Contents lists available at ScienceDirect

Organic Electronics

journal homepage: http://www.elsevier.com/locate/orgel

Suppression of Ag migration by low-temperature sol-gel zinc oxide in the Ag nanowires transparent electrode-based flexible perovskite solar cells

Jiachen Kang [a,b], Kang Han [b], Xue Sun [b], Lianping Zhang [b], Rong Huang [b], Irfan Ismail [b], Zhenguo Wang [b], Changzeng Ding [b], Wusong Zha [b], Fangsen Li [b], Qun Luo [b,c,d,*], Yuanjie Li [a,**], Jian Lin [b,d], Chang-Qi Ma [b,d,***]

[a] School of Electronic Science and Engineering, Xi'an Jiaotong University, Xi'an, 710049, PR China
[b] Printable Electronics Research Center, Suzhou Institute of Nano-Tech and Nano-Bionics, Chinese Academy of Sciences (CAS), Suzhou, 215123, PR China
[c] State Key Lab of Silicon Materials, Zhejiang University, Hangzhou, 310027, PR China
[d] Suzhou Institute of Nano-Tech and Nano-Bionics Nanchang, Chinese Academy of Sciences, 298 Luozhu Road, Nanchang, 330200, PR China

ARTICLE INFO

Keywords:
Flexible perovskite solar cells
Ag nanowire electrode
Sol-gel ZnO
Ag migration
Bending resistance

ABSTRACT

Silver nanowires (Ag NWs) network is an excellent candidate as flexible transparent electrode applying in flexible perovskite solar cells, owing to their excellent electrical and optical properties. However, several problems including large surface roughness, chemical reaction between Ag and perovskite precursor, and migration of Ag limited the application in high performance perovskite solar cells. Aiming to solve these problems, the composite electrode combining the spray coated Ag nanowires and the low-temperature sol-gel zinc oxide was developed in this work. The optimized concentration and annealing temperature of sol-gel ZnO were 0.45 M and 150 °C. The introduction of zinc oxide with suitable concentration caused slight impact on the transmittance and sheet resistant of transparent composite electrode, and promoted mechanical and chemical stability in air relative to the pristine Ag NWs electrode. The use of the composite flexible electrode could decrease the surface roughness of the Ag NWs electrode, passivate the reaction of perovskite and silver electrode, and prevent the migration of Ag. As a consequence, the performance of the flexible device significantly improved from 9.51% to 13.12%. Under the AM 1.5G constant illumination, the optimization device has a remarkably improved stability than pristine device. This study demonstrates that spray Ag NWs as bottom electrode is suitable for flexible perovskite solar cells. Meanwhile, it's an effective method using sol-gel ZnO to construct composite electrode to promote the device performance and stability.

1. Introduction

In the past decade, perovskite solar cells (PVSCs) have attracted enormous attentions in the field of photovoltaics and power conversion efficiencies (PCEs) over 25.2% have been achieved [1–5]. The excellent performance of the perovskite solar cells could be due to the superior photoelectric property including long charge diffusion length, appropriate bandgap to absorb sunlight, large extinction coefficient and cheap raw materials and preparation process [6–10]. Meanwhile, PVSCs are highly comparable with low temperature solution process and flexible substrates. Recently, the flexible perovskite solar cells have achieved remarkable development on PEN/ITO substrate, with a highest PCE of 19.51% was reported [11].

In the flexible perovskite solar cells, ITO is widely used as a transparent conducting electrode (TCE) until now. However, ITO is not suitable for flexible cells due to their poor mechanical robustness [12]. Therefore, many research efforts have been made in developing flexible transparent electrode that is suitable to flexible device and solution process [12].

Besides ITO electrode, there are several flexible TCEs such as carbon

* Corresponding author. Printable Electronics Research Center, Suzhou Institute of Nano-Tech and Nano-Bionics, Chinese Academy of Sciences (CAS), Suzhou, 215123, PR China.
** Corresponding author.
*** Corresponding author. Printable Electronics Research Center, Suzhou Institute of Nano-Tech and Nano-Bionics, Chinese Academy of Sciences (CAS), Suzhou, 215123, PR China.
E-mail address: qluo2011@sinano.ac.cn (Q. Luo).

https://doi.org/10.1016/j.orgel.2020.105714
Received 22 December 2019; Received in revised form 29 February 2020; Accepted 1 March 2020
Available online 20 March 2020

nanotubes (CNT) [13,14], high conductive polymer [15,16] and metal electrode [17–19]. Among these flexible TCEs, silver nanowires network (Ag NWs) is an excellent candidate as flexible transparent electrode applying in flexible perovskite solar cells, owing to their excellent electrical and optical properties [20,21]. Ag NWs networks have been readily deposited using spin coating [22], spray coating [23,24] and ink-jet printing [25], and used as transparent electrode for the perovskite solar cells. Kang et al. [26] reported ultralight and flexible perovskite solar cells (PSCs) with second-step capillary printing orthogonal Ag NWs transparent electrodes, achieving an outstanding power-per-weight of 29.4 Wg^{-1} with a PCE of 12.85%. For the use the Ag NWs in the perovskite solar cell, there are several problems should be solved. Frist is the chemical reaction between $CH_3NH_3I_XCl_{3-X}$ and Ag electrode. Thus, it is reported that is necessary to modify the Ag NWs with metal oxide or graphene. Lee et al. [22] used a pinhole-free amorphous aluminum doped zinc oxide (a-AZO) protection layer to protect Ag NW. Jin et al. [27] prepared sol–gel ZnO protective layer and ALD-deposited TiO_2 to smooth and passivate surface, and achieved PCE of 17.11%. Besides the chemical reaction, a serious problem of Ag electrode is migration. It was reported that silver would diffuse through an organic transport layer into the perovskite layer. Meanwhile, light accelerates reactions between perovskites and metal because of the formation of the photogenerated holes oxidize halogens mobile halogen [28]. Liang et al. reported that Ag^+ will penetrate from Ag electrode into hole transporting layer (HTL) and react with iodine ions in perovskite, which will increase the defect density in HTL, leading to the degradation of device performance [29,30]. However, these works are almost about the migration issue of Ag from the evaporated top electrode to the underneath layer. Rare work was reported on the migration problem and the passivation method for the Ag transparent bottom electrode-based perovskite solar cells.

In this work, we aimed to solve the chemical reaction and Ag migration issue in the Ag NWs-based perovskite solar cells, and improve the performance and stability. Large-area Ag NWs electrode was fabricated through spray coating. Spray method is one of most simple and convenient way to fabricate a large area, high transmittance, low sheet resistance transparent conductive film. Low-temperature ZnO layer was utilized as a modifier to suppress the chemical reaction and Ag migration. We systematically optimized the thickness and morphology of zinc oxide layers through regulating concentrations and annealing temperature. The transmittance and sheet resistant show slight change after adding ZnO. With the modification of ZnO layer, the surface roughness of Ag NWs obviously decreased, and the silver migration was effectively protected as well. As a result, the power conversion efficiency (PCE) of the flexible perovskite solar cells significantly improved from 9.51% to 13.12%. Meanwhile, Secondary Ion Mass Spectrometry (SIMS) results proved the Ag migration from the bottom electrode to the perovskite and PCBM layers was suppressed by the ZnO layer, resulting in a remarkable improved stability than pristine device under continuous illumination condition. This study demonstrated that composite electrode with spray coated Ag NWs electrode and low-temperature ZnO layer is suitable for use in flexible perovskite solar cells.

2. Experimental section

2.1. Materials

Silver nanowires dispersed in deionized water and diluted to 1.4 mg/mL with isopropanol (IPA) were purchased from Naibotech company. The diameter and length of Ag nanowire are 30 nm and 20–30 μm, respectively. The zinc acetate was supplied by Aladdin Ltd. And the dimethoxy ethanol and ethanolamine were purchased by J&K Scientific Ltd and Adamas Reagent Co., Ltd respectively. The PEDOT: PSS (AI 4083) was purchased from Heraeus Ltd. Lead chloride ($PbCl_2$, 99%), Lead iodide (PbI_2, 99%), Methylammonium Iodide (MAI, 99.5%), were purchased from Xi'an Polymer Light Technology Corp. The (6,6)-phenyl-C_{61}-butyric acid methyl ester ($PC_{61}BM$) were bought from Sigma-Aldrich.

2.2. Fabrication of Ag NWs/ZnO composite electrode

The Ag NWs were fabricated on the top of PET substrates by spray method. The PET substrates were treated with ultraviolet-ozone (UVO) cleaner for 5 min. After that, the Ag NWs transparent electrodes were prepared on the PET substrates under environment conditions by spray-method (Hizenith AC300-1, Hizenith Robot (Suzhou) Co., Ltd.). The nozzle moves at a speed of 16 mm/s, and the substrate is annealed at 53 °C. The ZnO sol-gel precursor was prepared through dissolving zinc acetate in dimethoxy ethanol, with a small amount of ethanolamine as stabilizer, and followed by stirring overnight. Then the sol-gel ZnO precursor solution with different concentration was deposited on the top of Ag NWs through spin-coating method at 2000 rpm for 30 s to form a composite electrode. After that, the composite electrode film, was annealed on a hot plate at 150 °C for 0.5 h.

2.3. Fabrication and measurement of the flexible perovskite solar cells

The $MAPbI_xCl_{3-x}$ active layer was fabricated through one step anti-solvent method. The detailed fabrications process was described as follow: PEDOT: PSS (4083) hole transport layer was spin-coated at 2000 rpm for 45s on the PET/Ag NWs/ZnO. Then, the film was annealed at 130 °C for 10 min and transferred into the N_2 -filled glove box to deposit perovskite film and $PC_{61}BM$ layers. Before that the perovskite precursor solution was prepared by dissolving 103.3 mg of methylamine iodide (MAI), 310.10 mg of lead iodide (PbI_2) and 9.72 mg of lead chloride ($PbCl_2$), which were stirred in the mixture of $C_4H_6O_2$ (GBL) C_2H_6OS (DMSO) (7:3 v/v) at 50–60 °C for at least 2 h. The perovskite films were deposited by a consecutive two-step spin-coating process at 1000 rpm for 10 s, and at 4000 rpm for 30 s. During the second-step spin-coating at 17 s, 400 μL antisolvent anhydrous chlorobenzene was dropped onto the center of the film. After that the perovskite layer was annealed at 100 °C for 10 min. After cooling to room temperature, the $PC_{61}BM$ solution (20 mg/mL in chlorobenzene) was spin- coated onto the perovskite film at 1000 rpm for 45 s. Finally, 100 nm-thick Al was deposited on the $PC_{61}BM$ film through a shadow mask under a vacuum of 10^{-5} torr.

The transmittance and absorption spectra were measured by the Lamada 750 UV–vis–NIR Spectro-photometer (PerkinElmer). The micrograph was investigated by cold field emission Scanning Electron Microscope (SEM, S-4800). Photoluminescence was tested by steady-state and transient-state fluorescence spectrometer (JY Fluorolog-3-Tou). Surface morphology was observed by using an Atomic Force Microscopy (AFM, Dimension 3100). The ionic migration after aging was investigate by Time of Flight Secondary Ion Mass Spectrometry (SIMS). The *J–V* characteristics of devices were measured in glove box using a Keithley model 2400 source measurement unit. The external quantum efficiency (EQE) of cell was measured as a function of wavelength, under simulated one sun operation conditions.

3. Result and discussion

It is well known that transmittance and sheet resistance are two basic parameters for a transparent conductive film. Therefore, the effect of ZnO on transmittance and sheet resistance of transparent electrodes was comprehensively investigated. In this study, we firstly investigated the influence of ZnO annealing temperature and precursor concentration on the transmittance and sheet resistance of the transparent electrode. Fig. 1(a) shows the photo of large area Ag NWs flexible transparent electrode fabricated by spray method. The sheet resistance of Ag NWs/ZnO(0.45 M) at different annealing temperatures of sol-gel ZnO was showed in Fig. 1 (b). It exhibited that the sheet resistance of the composite electrode increased gradually as the annealing temperature decreases. A lowest sheet resistance of 29.5 ± 0.70 Ω/sq was obtained

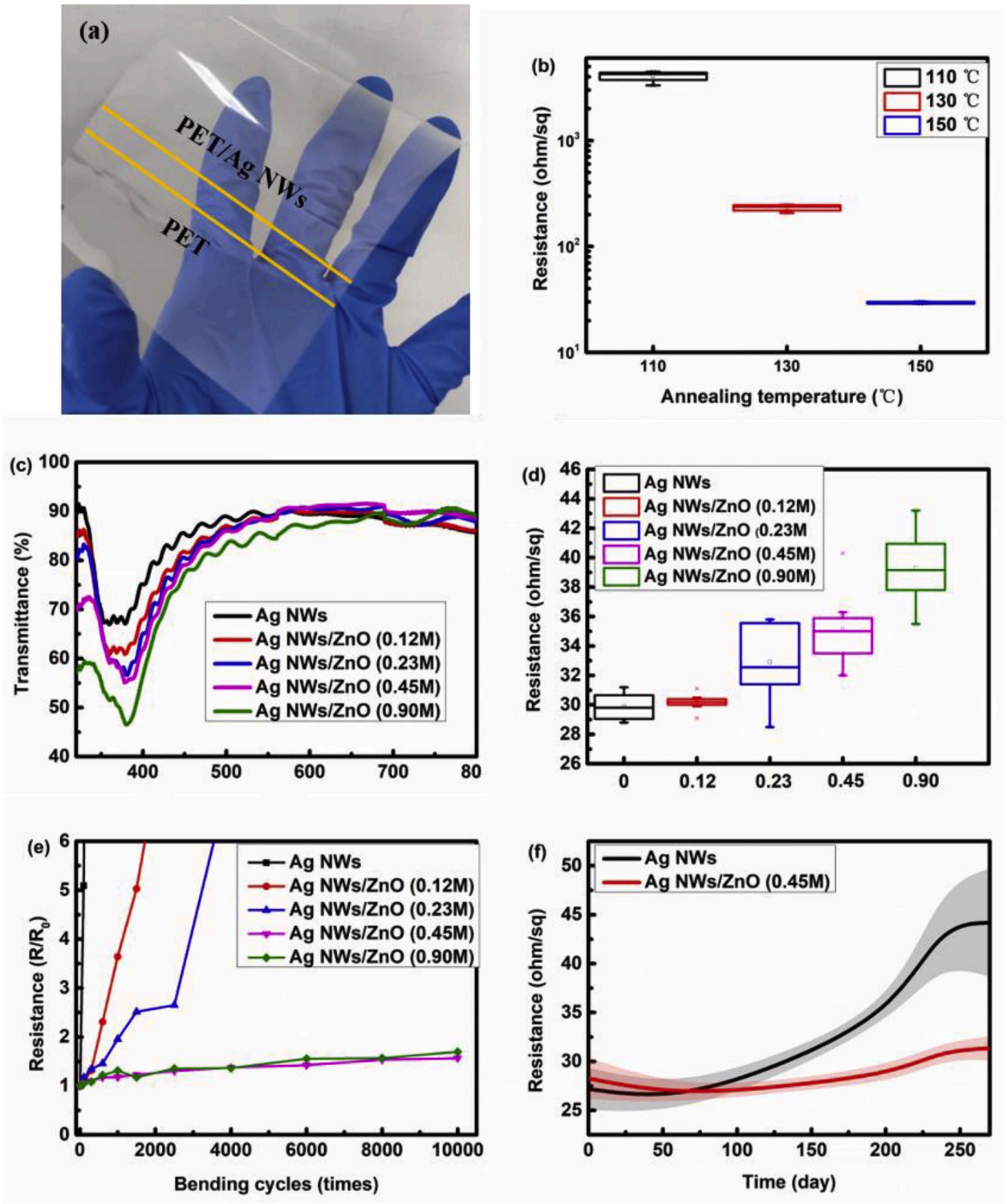

Fig. 1. (a) Photograph of large-area transparent conducting film through spray-coating method (b) The sheet resistance of Ag NWs/ZnO(0.45 M) composite electrode under different annealing temperatures. (c) Transmittance spectra of composite electrode with different modifications of ZnO. (d)Sheet resistance of the Ag NWs/ZnO films with different concentrations of ZnO. (e) Bending property of the composite electrode. (f) Evolution of the sheet resistance of composite electrode during long-term storage in air.

when the annealing temperature is 150 °C. We know the PET substrate can bear high temperature annealing, so 150 °C was chosen to fabricate ZnO layer in this work. The XRD patterns and AFM images of the ZnO layer with different annealing temperatures were demonstrated in Fig. S1 and Fig. S2. For the XRD data, we found all the samples didn't show obvious diffraction peaks corresponding to ZnO, and only a wide diffraction peak at around 28° was observed, indicating the sol-gel ZnO layers were amorphous after annealing at temperatures from 110 °C to 150 °C. These results were reasonable since the crystallinity temperature of the sol-gel ZnO was above 200 °C [31]. The AFM images of the ZnO films showed the root-mean-square roughness (RMS) of ZnO film is 0.58, 0.53, and 0.61 nm for the samples that annealed under 110 °C, 130 °C,

and 150 °C, respectively. These results demonstrated the ZnO films annealed at 110 °C, 130 °C, and 150 °C had similar surface morphology and crystallinity. So, the differences of sheet resistance for the Ag NWs/ZnO composite electrode caused by annealing temperatures might be originated from the difference of composites. For the ZnO films annealed at higher temperature, both the precursor solvents and raw materials could be removed or transformed to amorphous ZnO, while the films annealed under low temperature contained more precursor solvents and raw materials. Consequently, the conductivity of the Ag NWs/ZnO composite electrode improved gradually with the increasing of the annealing temperatures. Fig. 1 (c) shows the influence of ZnO concentration on the transmittance and sheet resistance of the composite electrodes. For the Ag NWs flexible electrode without modification, it showed a transmittance of 90% at 550 nm and average sheet resistance of 28 Ω/sq. After introducing a zinc oxide modification layer on the top of Ag NWs network, the transmittance in the region of wavelength from 350 to 400 nm significantly decreased, for which is the absorption peak position of zinc oxide. Among the visible light region from 400 to 800 nm, the transmittance of composite film was only slightly decreased. Overall, the composite electrodes showed an average visible transmittance around 84%. As shown by Fig. 1(d), we found the average sheet resistance increased gradually from 28 to 40 Ω/sq with the increase of ZnO concentration. The thickness of ZnO with different concentrations was tested and showed in Table S1. Herein, the thicknesses of the ZnO layer were estimated through testing the ZnO films that deposited on the top of glass substrates. Since the sol-gel ZnO would partly permeate into the Ag NWs networks (as shown by the AFM images), the measured thickness on the glass substrates would be not consistent with the situation in the Ag NWs/ZnO composite electrodes. Nevertheless, a relationship between the concentration and the thickness could be provided. As showed by Table S1, the optimized thickness of ZnO, corresponding to the concentration of 0.45 M, was about 80 ± 10 nm. With the concentration increasing to 0.90 M, the thickness of ZnO increased to 215 ± 20 nm approximately. The sheet resistance of composite electrode is mainly dominated by the Ag NWs network. Thus, introducing ZnO only caused slight change of the sheet resistance. All the sheet resistances were below 50 Ω/sq, which were nearly comparative to the flexible ITO electrode. Based on the average transmittance around 84% and average sheet resistance of 30–50 Ω/sq, it is feasible to use such Ag NWs/ZnO composite electrode in the flexible perovskite solar cells. Furthermore, we explored the bending resistant testing of Ag NWs flexible electrode, and the sheet resistance of the electrodes after different bending cycles were tested. As showed in Fig. 1 (e), the sheet resistance of pristine Ag NWs dramatically increased to 574.2 Ω/sq, which was 20 times of the initial value only after 300 bending experiments. The poor mechanical properties of the pristine electrode were due to the poor adhesion between the silver wire and the substrate. But the bending resistance significantly improved after introducing ZnO film, which might be because the modification of ZnO inhibited the movement of silver wires during bending. The composite electrode can maintain an average sheet resistance of 44.3 Ω/sq after 10000 bending cycles with a bending radius of 7.5 mm. We also monitored the long-term air staibilty of Ag NWs and Ag NWs/ZnO(0.45 M) electrode during 270-day's storage. As showed in Fig. 1 (f), it is obivous that the resistance of Ag NWs electrode increased from the initial 27.2–44.2 Ω/sq, and that of the Ag NWs/ZnO(0.45 M) composite eletrode increased from the initial 28.3–31.3 Ω/sq. This result indicated the air chemcial stabiltiy of Ag NWs electrode improved through sol-gel ZnO modification, which might be due to the prevetion of Ag oxidation. Based on these reuslts, we can conclude that the introduction of ZnO protected the silver nanowire and improve the air stability.

The surface morphology of the bottom electrode is crucial for the quality of upper film and even for the performance of the device. The surface morphology of corresponding film has been investigated by atomic force microscope (AFM) images (as showed in Fig. 2(a-h)). As shown in these images, the Ag nanowires networks were clearly observed in the pristine Ag NWs electrode. For the composite electrode with low concentration ZnO layer, the Ag NWs networks became unclearly in comparison with the pristine Ag NWs, suggesting the covering of ZnO on Ag NWs. However, because of low concentration, ZnO would mainly permeate into the pores of the Ag NWs networks. Thus, the surface of the Ag NWs was not completely covered by ZnO. In case of ZnO layer with higher concentration, ZnO would not only permeate into the networks of Ag NWs, but also cover on the top. As showed in Fig. 2(e), ZnO film covered well on the Ag NWs network with concentration of 0.45 M. As ZnO concentration increased up to 0.90 M, the wrinkle structure was observed on the film surface, which was the typical morphology of sol-gel ZnO films [32,33]. According to the AFM images, the root-mean-square roughness (RMS) of the Ag NWs film is 21.2 nm. This result indicated the spray-coated Ag NWs electrode is relatively rough, which is the reason of low performance and device short circuit. After adding ZnO, the roughness of composite film obviously reduced to 8.5 nm (RMS) for the Ag NWs/ZnO (0.23 M) composite electrode. With further increasing the ZnO precursor concentration, the roughness of composite film increases slightly to 10.7 nm for Ag NWs/ZnO (0.45 M), which was due to the formation of wrinkle on the ZnO surface. These results illustrated the modification by ZnO with suitable concentration can decrease the roughness of composite electrode, which is a favorable interfacial contact layer to gain a better interface contact and enable the formation of the up film. Fig. 2(i)–(l) demonstrate the schematic diagram of composite electrode with different ZnO concentrations.

In order to further explore the impact of surface morphology of composite electrode to the film formation properties of the upper film, the contact angle of water on the flexible electrode has been investigated. Fig. 3 shows the contact angle of water on the different composite film. It's obvious that the contact angle on the PET/Ag NWs is larger than others films that with a ZnO layer on the top of Ag NWs. The much larger contact angle between water and the pristine Ag NWs electrode could be ascribed to the direct contact of water and the PET substrate. Because Ag NWs formed a random network structure, water can penetrate into the silver wire and directly contact with the substrate surface. Thus, the contact angle between water and the pristine Ag NWs electrode was around 53°. As gradual increasing of ZnO concentration, the contact angle gradually decreased from 53° to 35°. One reason is the surface roughness of the film increases as the concentration of ZnO increases. Another reason is the improved coverage of Ag NWs by ZnO films, which can prevent the water permeation and avoid direct contact of water and PET substrate. Herein, the reduced contact angle between water and the flexible electrode would be favorable for the formation of PEDOT: PSS film on the top of the flexible electrode, and consequently improve the film quality of the perovskite layer, since PEDOT: PSS is aqueous.

With the modification of Ag NWs by the ZnO interface layer, flexible perovskite solar cells with architecture of PET/Ag NWs/ZnO/PEDOT: PSS/perovskite/$PC_{61}BM$/Al were fabricated. The device structure diagram and the energy level of the device are shown in Fig. 4(a). The energy levels of the perovskite and PCBM layers were given according to the references. [34] The *J-V* characteristics and EQE spectra of the flexible solar cells are showed as Fig. 4(b). The performance parameters of these devices were listed in Table 1. Notably, the reference device with pristine Ag NWs electrode yields a best power conversion efficiency (PCE) of 10.14% and an average PCE of 9.51%. For the optimized performance, a J_{SC} of 17.75 mA cm^{-2}, a V_{OC} of 1.01 V, and FF of 57% were obtained from reverse scan. With the insertion of a ZnO modification layer, the device performance improved gradually first and then decrease, with the concentration of 0.45 M as the saturation value. As an optimized performance using Ag NWs/ZnO composite electrode, an efficiency of 13.12% was observed with the ZnO concentration of 0.45 M. A V_{OC} of 1.02 V, J_{SC} of 17.56 mA cm^{-2}, and FF of 75% were observed in reverse scan. Obviously, the performance enhancement for the Ag NWs/ZnO composite electrode-based device was mainly caused by

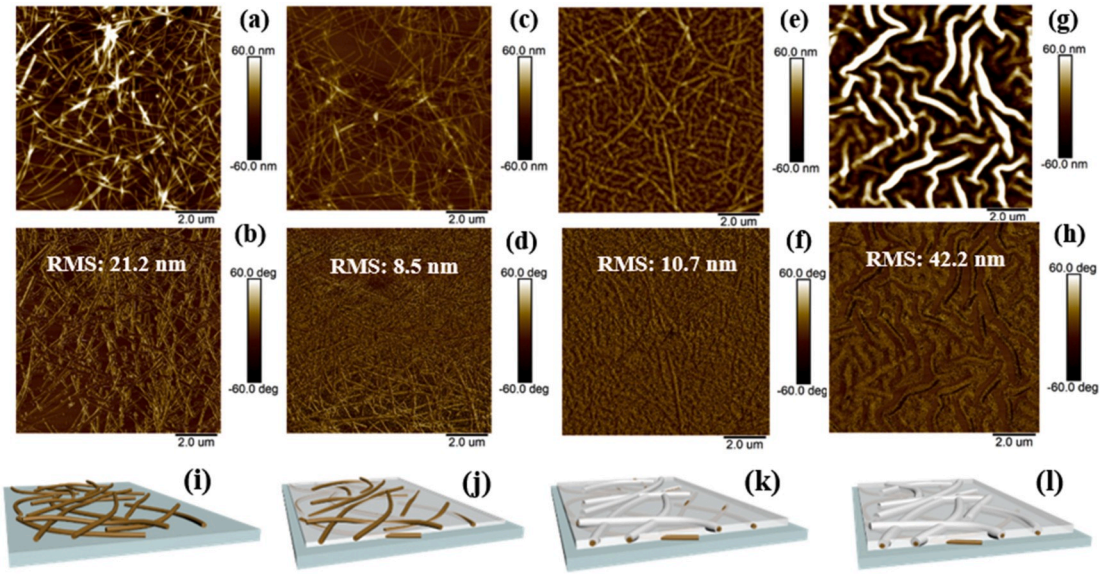

Fig. 2. The AFM morphology image and phase diagram and corresponding composite electrode schematic of (a) (b) (i) Ag NWs, (c) (d) (j) Ag NWs/ZnO(0.23 M), (e) (f) (k) Ag NWs/ZnO(0.45 M), (g) (h) (l) Ag NWs/ZnO(0.90 M) films.

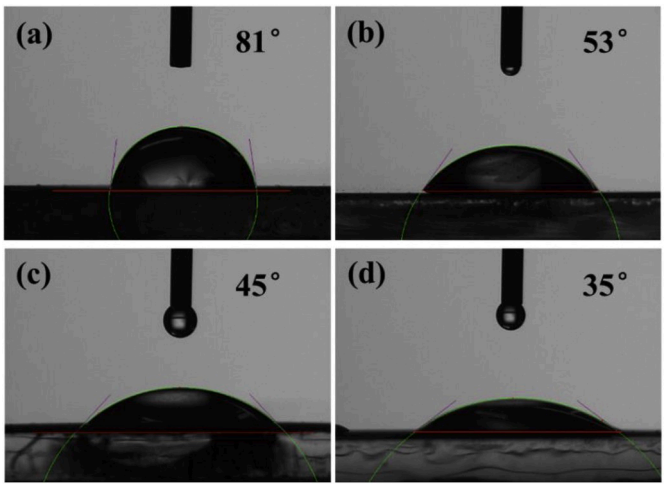

Fig. 3. The photographs a drop of water on the top of (a)Ag NWs, (b) Ag NWs/ZnO(0.23 M), (c) Ag NWs/ZnO(0.45 M), and (d) Ag NWs/ZnO(0.90 M).

improvement of FF. As shown in Table 1, it was found the improvement of FF for the Ag NWs/ZnO-based device could be attributed to the reduced series resistance. For the pristine Ag NWs electrode and the Ag NWs/ZnO composite electrode with low ZnO concentration, the devices exhibited a series resistance of 19.5 and 10.2 Ωcm^2. In contrast, the series resistances of the devices with Ag NWs/ZnO (0.45 M) and Ag NWs/ZnO (0.90 M) electrodes decreased to around 7.7 Ωcm^2. Therefore, better interface contact and superior charge transfer in Ag NWs/ZnO-based device could be expected. The photoelectric current images of reference and champion device have been tested by light-beam-induced-current (LBIC) mapping system (Fig. S3). The result shows that, compared with reference one, the distribution of photocurrent is more uniform. In addition, the J-V curve of forward and backward scans for optimized device was showed in Fig. S4. The result showed that the introduction of ZnO does not increase the hysteresis effect of the device. The device parameter of V_{OC}, J_{SC}, FF are similar between reverse and forward scan. The reference device with ITO electrode gave a J_{SC} of 18.37 ± 0.31 mA cm^{-2}, a V_{OC} of 1.03 ± 0.01 V, and FF of 0.74 ± 0.01. And a best PCE of 14.23% and an average PCE of 14.02% were obtained from reverse scan. The lower performance of the PET/Ag NWs/ZnO electrode-based solar cells may be caused by the higher surface roughness and sheet resistance compared to ITO electrode. The external quantum efficiency (EQE) spectra showed the introducing the ZnO caused slight decrease in short-wavelength-range due to the absorption of ZnO, which was in good agreement with the absorption spectra. Moreover, the steady-state photocurrent and efficiency of the champion device was conducted at the maximum power point up to 300 s (Fig. 4(d)). The PCE of the device with ZnO (0.45 M) stabilized at 13.10%, which was close to the value obtained from the *J–V* measurement. The histogram of PCE with 32 devices exhibits an excellent performance by introducing ZnO (Fig. 4(e)). Devices without ZnO modification have an efficiency distribution between 7% and 10% and an average efficiency of 8.65%. After introducing ZnO modification layer, the device with ZnO layer have an efficiency distribution between 11% and 13% and an average efficiency of 12.37%.

In order to further explore the reason of performance improvement by introducing ZnO interface layer, the characterization of the perovskite film on different flexible electrodes was measured. Fig. 5(a)-(c) show the top-view scanning electron microscope (SEM) images of the perovskite films on the pure Ag NWs and Ag NWs/ZnO composite electrodes. In the SEM image, we found both the films on the top of Ag NWs and Ag NWs/ZnO composite electrodes have darker grain and brighter grain, which could be ascribed to the perovskite and PbI_2 phase, respectively. The grain size of the $MAPbI_xCl_{3-x}$ phase is approximately 300 nm, and the lead iodide phase has a grain size of about 200 nm and a width of about 100 nm. The result showed that there were no significance changes of perovskite crystal size after introducing ZnO on Ag NWs. In addition, the SEM image of perovskite film on the pristine Ag NWs electrode showed several small particles distribute in the perovskite film, while no such particle was observed in perovskite film that deposited on the top of Ag NWs/ZnO composite electrode. In combination with related literature, these small nanoparticles might be ascribed to the binary iodine. The XRD patterns of the PVSC films were showed in supporting information Fig. 5(d). The typical diffraction peaks at 12.7°and 14.1°corresponded to the typical plane of PbI_2 and PVSK, respectively. Nevertheless, the broad diffraction peak over 20–30°was attributed to the PET substrate [35,36]. Notably, the diffraction of PVSK film with PET/Ag NWs/ZnO composite electrode was slightly higher than the PET/Ag NWs w/o ZnO. Meanwhile, we can obtain the similar thickness of PVSK due to the same UV–vis absorption

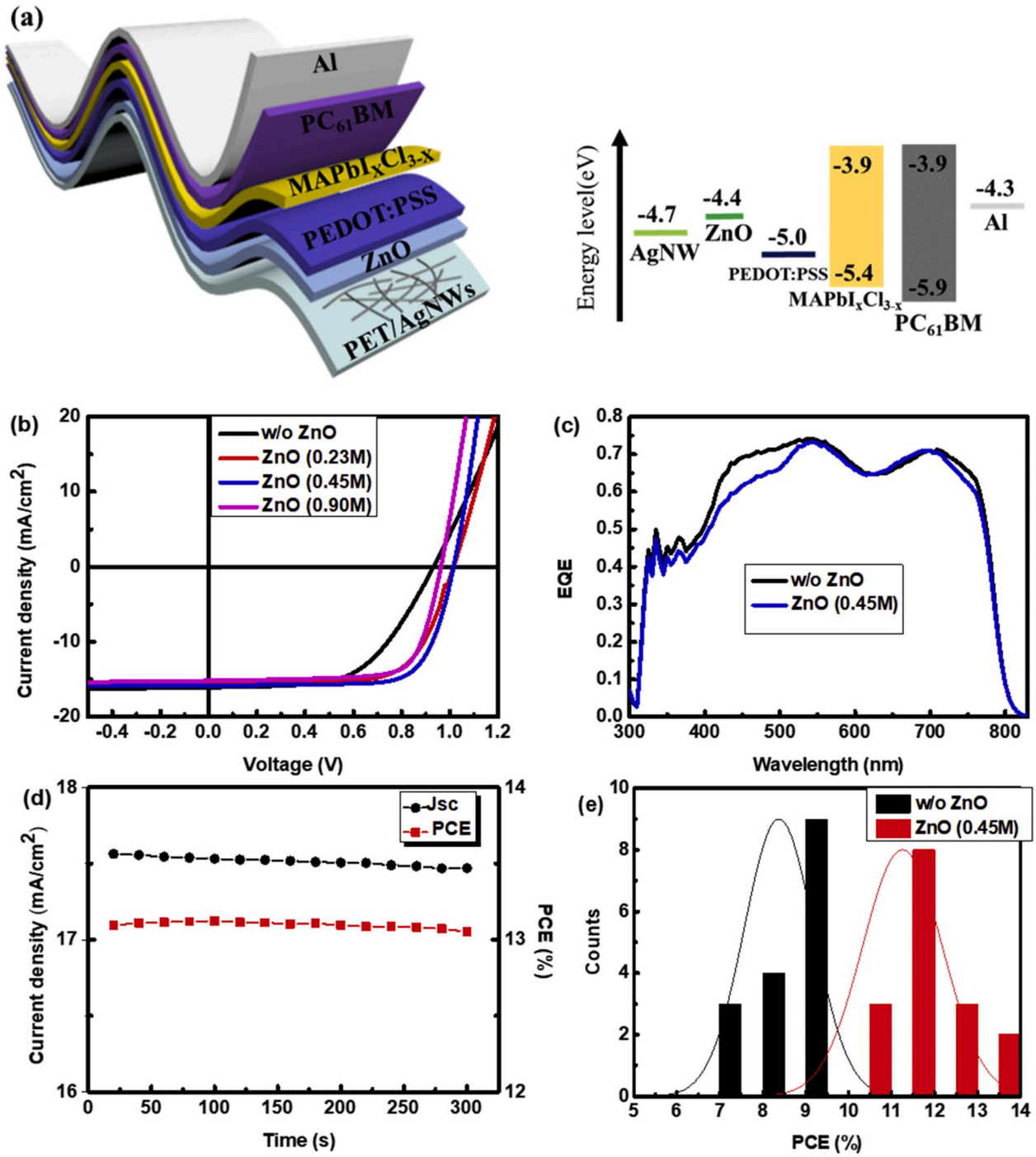

Fig. 4. (a) The device structure diagram and the energy level distribution, (b) The current density–voltage characteristics, (c) external quantum efficiency, (d) Steady-state photocurrent and output PCE at the maximum power point, (e) The PCE histogram of 32 PVSCs.

Table 1
Device performance of the perovskite solar cells with glass/ITO electrode and PET/Ag NWs flexible electrodes with different concentrations of ZnO.

Concentration (Mol/L)	V_{OC}(V)	J_{SC}(mA/cm^2)	FF	PCE (%)	Best PCE	R_s (Ωcm^2)	R_{sh} (Ωcm^2)
w/o	1.00 ± 0.01	17.61 ± 0.14	0.53 ± 0.04	9.51 ± 0.63	10.14	19.2	1952
0.23	1.03 ± 0.01	17.53 ± 0.09	0.69 ± 0.01	12.58 ± 0.07	12.65	10.5	2692
0.45	1.01 ± 0.01	17.48 ± 0.08	0.74 ± 0.01	13.06 ± 0.06	13.12	7.7	5378
0.90	0.96 ± 0.01	16.42 ± 0.20	0.74 ± 0.01	11.74 ± 0.10	11.84	7.3	2191
ITO w/o	1.03 ± 0.01	18.37 ± 0.31	0.74 ± 0.01	14.02 ± 0.29	14.23	6.4	1739

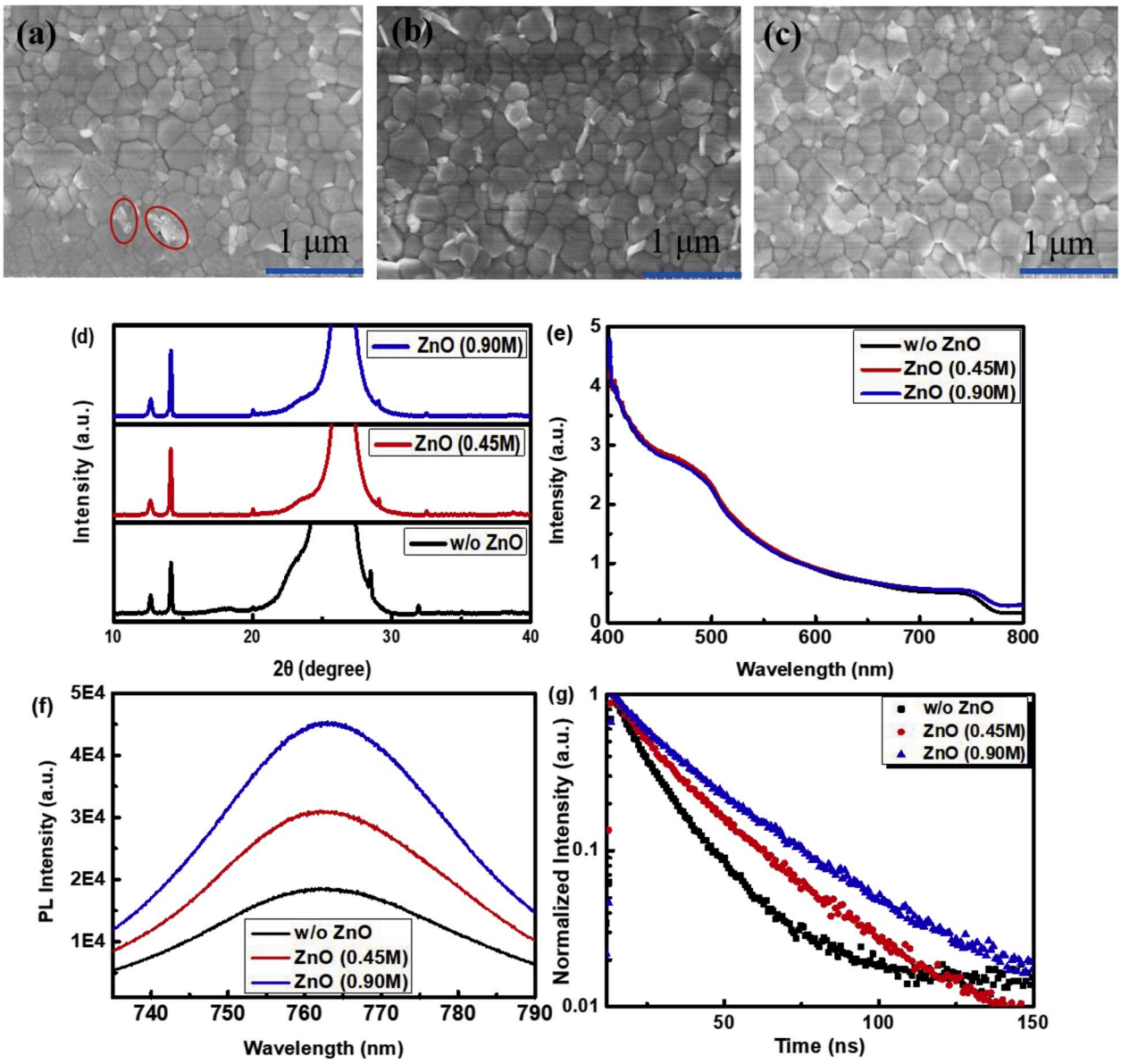

Fig. 5. Top view SEM image of perovskite film (a) w/o ZnO, (b) ZnO(0.45 M), (c) ZnO(0.90 M), (d) The XRD patterns of the PVSK film on the Ag NWs electrode w/o ZnO and on the ZnO layers, (e) UV–vis absorption spectra, (e) steady-state PL spectra, and (f) time-resolved PL spectra of the perovskite films on the pristine Ag NWs and Ag NWs/ZnO composite electrodes.

result. Therefore, the enhanced intensity of the diffraction peaks indicated improved crystallinity of PVSK film.

The UV–vis absorption spectra of the perovskite films on Ag NWs and Ag NWs/ZnO composite electrode were showed in Fig. 5(e). It exhibits slight changes in absorption spectra, indicating the same thickness of perovskite film. Further, the steady and transient photoluminescence (PL) spectra of these perovskite films on the flexible electrode/PEDOT: PSS were measured and showed in Fig. 5(f). A stronger PL intensity of $MAPbI_xCl_{3-x}$ film was observed after introducing ZnO interfacial layer, which suggested that the quality of the film was improved after introducing ZnO. Fig. 5(g) showed the transient PL spectra of the perovskite films. According to the transient PL spectra, we can calculate the average carrier lifetime of the perovskite films through curves fitting with double exponential decay function. The pristine $MAPbI_xCl_{3-x}$ films on the Ag NWs/PEDOT: PSS exhibited a relatively short lifetime of 15.0 ns, whereas lifetime of $MAPbI_xCl_{3-x}$ on the Ag NWs/ZnO/PEDOT: PSS increased to 26.7 and 28.5 ns for the samples with 0.45 M and 0.90 M ZnO. The corresponding details was summarized in the supporting information (Table S2). According to the XRD patterns of the PVSK film, we can conclude that the enhanced crystallinity is the reason of the increased PL intensity and carrier lifetime of the perovskite films, as showed by the PL and transient PL spectra.

We monitored the long-term photostability of unencapsulated $MAPbI_xCl_{3-x}$ with Ag NWs and Ag NWs/ZnO composite electrodes under continuous illumination in N_2 filled glovebox. The evolution of performance is showed in Fig. 6(a–d). The result showed a significant improvement of stability of the Ag NWs/ZnO composite electrode-based device relative to the perovskite solar cells with pristine Ag NWs electrode. For the device on the pristine Ag NWs electrode, the device nearly could not work after only 30 h storage under continuous illumination. Such a quick degradation of performance was mainly due to the decay of J_{SC} and FF. While the device with Ag NWs/ZnO composite electrode remained around 50% of the initial efficiency after 160 h's continuous illumination. To further verify the improvement of the stability, the Secondary Ion Mass Spectrometry (SIMS) has been tested for the aged devices. By analyzing the changes of Al, C, Pb, Ag element, the

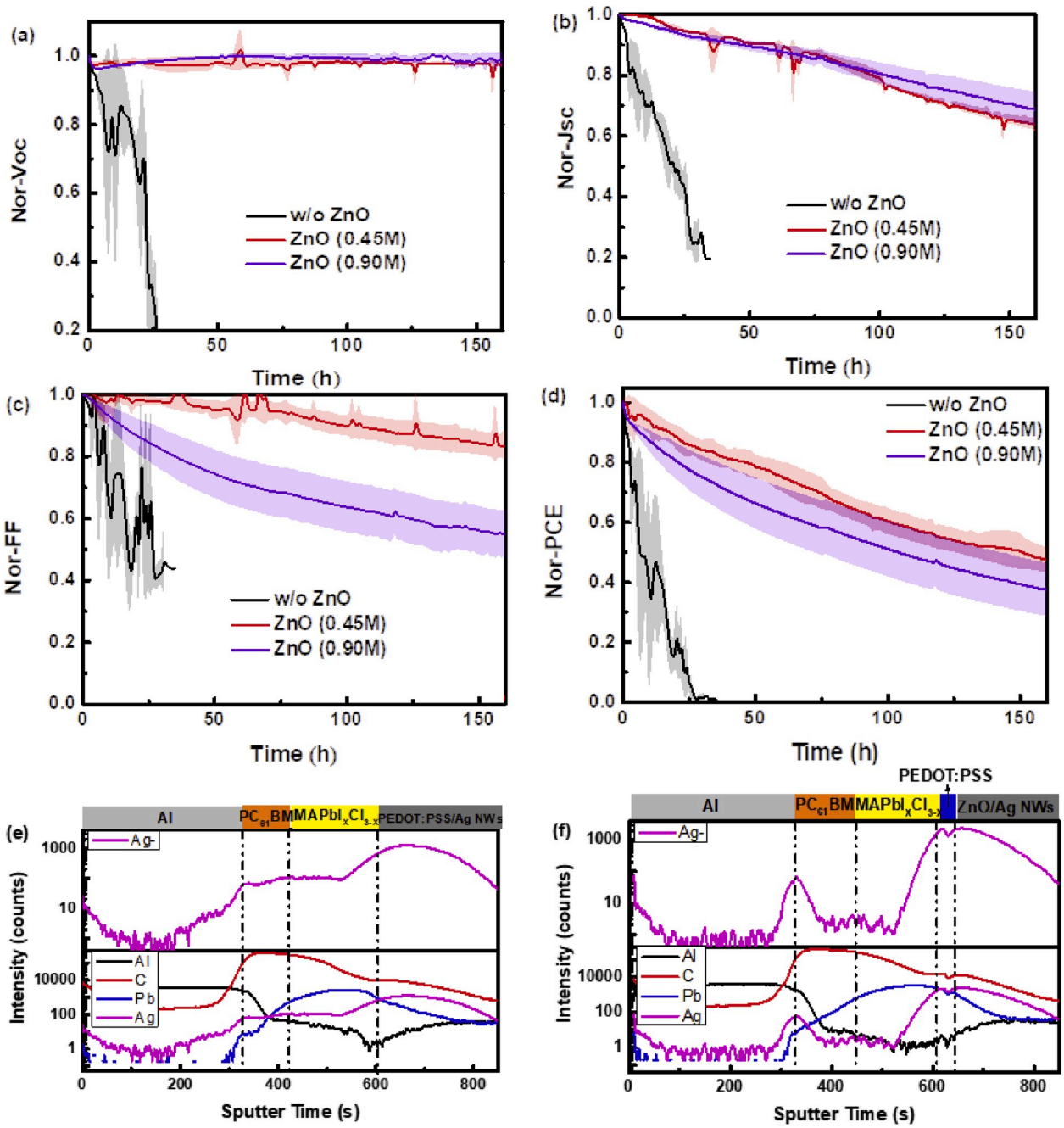

Fig. 6. The evolution of (a)V_{OC}, (b) J_{SC}, (c)FF, (d) PCE for the perovskite solar cells during long-term continuous illumination. The Secondary Ion Mass Spectrometry (SIMS) results of aging devices: (e) w/o ZnO, (f) ZnO (0.45 M).

corresponding interfaces of Al, $PC_{61}BM$, $MAPbI_xCl_{3-x}$, PEDOT: PSS and Ag NWs/ZnO layers were determined. The changes of the contents of S, Pb, and I element in different devices were showed in Fig. S5. Similar results were observed in the devices with Ag NWs and Ag NWs/ZnO electrodes, indicated the introduction of ZnO did not cause change of elemental distribution among the devices. However, as showed in Fig. 6 (c and d), the distribution of Ag elements was quite different in devices with pristine Ag NWs and Ag NWs/ZnO composite electrode. The aged device without ZnO layer showed strong signal of silver both in the $MAPbI_xCl_{3-x}$ and PCBM layer, suggesting the migration of Ag from the bottom electrode to both of the PVSC and PCBM layers. For the perovskite solar cells with Ag electrodes, several works have reported the serious reaction issue between the perovskite layer and Ag electrode, which has been mainly attributed to as an iodine migration induced process [37–39]. As a result, AgI would formed, and resulted in the degradation of the perovskite solar cells [28,40]. This work demonstrated silver could migrate into perovskite layer as well. Similarly, the migration of Ag in to the perovskite layer might cause the degradation of the solar cells due to the reaction of Ag and the perovskite layer. Herein, the suppression of silver migration by sol-gel ZnO layer is mainly a physical effect due to the robust protection effect. Similarly, graphene [41] and sol-gel AZO [22] have been reported in the previous works. While for the device with Ag NWs/ZnO composite electrode, Ag signals were quiet low in the perovskite and PCBM layers. In order to further confirm the silver production process, we monitored the SIMS results of the fresh device without a ZnO modifier, as showed in Fig. S6. The result demonstrated that the fresh device has no silver signal in $MAPbI_xCl_{3-x}$ and PCBM layer. Based on these results, we can conclude that silver

could diffuse from the bottom Ag NWs electrode into the perovskite and PCBM layers during long-time aging period. However, the cover of the Ag NWs by ZnO could effectively prevent the Ag migration from the bottom electrode in the upper layers. Therefore, the significant improvement of the long-term stability through modifying Ag NWs with ZnO could be ascribed to the passivation of Ag migration by the sol-gel ZnO layer. In our previous report, we found the high conductive PEDOT:PSS (PH1000) assisted electrochemical corrosion of Ag electrode during the deposition process [34]. Though herein the PH1000 layer was absent in the device structure, electrochemical reaction might still occur during long-term degradation, which leads to the oxidation of Ag atoms to Ag^{+}. Then, the migration of Ag^{+} into the perovskite and PCBM layer caused the quick degradation of J_{SC} and FF. We also investigated the mechanical stability of device during 4000 times bending cycles with 7.5 mm bending radius (Fig. S7). Compared to pristine perovskite, the result shows the device with ZnO also maintained 80% of the initial efficiency after 4000 times bending cycles and the reference device remained only 60% of the initial efficiency.

4. Conclusion

In summary, large-area flexible transparent Ag NWs networks electrode were fabricated through spray coating, and composite electrode combining Ag NWs and low-temperature sol-gel ZnO layer was developed for use in flexible perovskite solar cells. The modification of Ag NWs electrode by sol-gel ZnO film layer caused the slight influence on the transmittance and sheet resistance of the electrode, but significantly improved the mechanical properties. The reduced surface roughness and effective surface protection of sol-gel ZnO caused significant improvement in the device performance. Meanwhile, ZnO interface layer acted as a protecting film which can dramatically restrain the diffusion of Ag, improving the continuous illumination stability. This work provided a route to improve the performance and stability of flexible perovskite solar cells based on the printed Ag NWs electrode.

Declaration of competing interest

The authors declared that they have no conflicts of interest to this work entitled “Suppression of Ag Migration by Low-Temperature Sol-Gel Zinc Oxide in the Ag Nanowires Transparent Electrode -Based Flexible Perovskite Solar Cells”.

Acknowledgements

The work is financially supported by Natural Science Foundation of Jiangsu Province (BK20181197), Natural Science Foundation of Jiangxi Province (20181BAB206017), Youth Innovation Promotion Association, CAS (2019317), National Natural Science Foundation of China (51773224), Visiting Scholar Foundation of State Key Lab of Silicon Materials, Zhejiang University (SKL2018-04), Suzhou Science and Technology Project (SYG201735), the Ministry of Science and Technology of China (2016 YFA0200700). Vacuum Interconnected Nanotech Workstation, Suzhou Institute of Nano-Tech and Nano-Bionics, Chinese Academy of Sciences (CAS).

Appendix A. Supplementary data

Supplementary data to this article can be found online at https://doi.org/10.1016/j.orgel.2020.105714.

References

[1] A. Kojima, K. Teshima, Y. Shirai, T. Miyasaka, Organometal halide perovskites as visible-light sensitizers for photovoltaic cells, J. Am. Chem. Soc. 131 (2009) 6050–6051, https://doi.org/10.1021/ja809598r.
[2] H.S. Kim, C.R. Lee, J.H. Im, K.B. Lee, T. Moehl, A. Marchioro, S.J. Moon, R. Humphry-Baker, J.H. Yum, J.E. Moser, M. Grätzel, N.G. Park, Lead iodide perovskite sensitized all-solid-state submicron thin film mesoscopic solar cell with efficiency exceeding 9%, Sci. Rep. 2 (2012) 591, https://doi.org/10.1038/srep00591.
[3] M.M. Lee, J. Teuscher, T. Miyasaka, T.N. Murakami, H.J. Snaith, Efficient hybrid solar cells based on meso-superstructured organometal halide perovskites, Science 80 (2012) 643–647, https://doi.org/10.1126/science.1228604, 338.
[4] P. Docampo, J.M. Ball, M. Darwich, G.E. Eperon, H.J. Snaith, Efficient organometal trihalide perovskite planar-heterojunction solar cells on flexible polymer substrates, Nat. Commun. 4 (2013) 2761, https://doi.org/10.1038/ncomms3761.
[5] NREL, Research cell efficiency records. http://www.nrel.gov/ncpv/, 2014. https://Pvdpc.Nrel.Gov/. Accessed July 2019.
[6] C.C. Stoumpos, C.D. Malliakas, M.G. Kanatzidis, Semiconducting tin and lead iodide perovskites with organic cations: phase transitions, high mobilities, and near-infrared photoluminescent properties, Inorg. Chem. 52 (2013) 9019–9038, https://doi.org/10.1021/ic401215x.
[7] H.J. Snaith, Perovskites: the emergence of a new era for low-cost, high-efficiency solar cells, J. Phys. Chem. Lett. 4 (2013) 3623–3630, https://doi.org/10.1021/jz4020162.
[8] J.H. Noh, S.H. Im, J.H. Heo, T.N. Mandal, S. Il Seok, Chemical management for colorful, efficient, and stable inorganic-organic hybrid nanostructured solar cells, Nano Lett. 13 (2013) 1764–1769, https://doi.org/10.1021/nl400349b.
[9] F. Hao, C.C. Stoumpos, R.P.H. Chang, M.G. Kanatzidis, Anomalous band gap behavior in mixed Sn and Pb perovskites enables broadening of absorption spectrum in solar cells, J. Am. Chem. Soc. 136 (2014) 8094–8099, https://doi.org/10.1021/ja5033259.
[10] J. Zhao, Y. Deng, H. Wei, X. Zheng, Z. Yu, Y. Shao, J.E. Shield, J. Huang, Strained hybrid perovskite thin films and their impact on the intrinsic stability of perovskite solar cells, Sci. Adv. 3 (2017), https://doi.org/10.1126/sciadv.aao5616 eaao5616.
[11] K. Huang, Y. Peng, Y. Gao, J. Shi, H. Li, X. Mo, H. Huang, Y. Gao, L. Ding, J. Yang, High-performance flexible perovskite solar cells via precise control of electron transport layer, Adv. Energy Mater. (2019) 1901419, https://doi.org/10.1002/aenm.201901419, n/a.
[12] J. Ahn, H. Hwang, S. Jeong, J. Moon, Metal-nanowire-electrode-based perovskite solar cells: challenging issues and new opportunities, Adv. Energy Mater. 7 (2017) 1602751, https://doi.org/10.1002/aenm.201602751.
[13] S. Seo, I. Jeon, R. Xiang, C. Lee, H. Zhang, T. Tanaka, J.W. Lee, D. Suh, T. Ogamoto, R. Nishikubo, A. Saeki, S. Chiashi, J. Shiomi, H. Kataura, H.M. Lee, Y. Yang, Y. Matsuo, S. Maruyama, Semiconducting carbon nanotubes as crystal growth templates and grain bridges in perovskite solar cells, J. Mater. Chem. A. 7 (2019) 12987–12992, https://doi.org/10.1039/c9ta02629k.
[14] Z. Li, S.A. Kulkarni, P.P. Boix, E. Shi, A. Cao, K. Fu, S.K. Batabyal, J. Zhang, Q. Xiong, L.H. Wong, N. Mathews, S.G. Mhaisalkar, Laminated carbon nanotube networks for metal electrode-free efficient perovskite solar cells, ACS Nano 8 (2014) 6797–6804, https://doi.org/10.1021/nn501096h.
[15] M. Kaltenbrunner, G. Adam, E.D. Głowacki, M. Drack, R. Schwödiauer, L. Leonat, D.H. Apaydin, H. Groiss, M.C. Scharber, M.S. White, N.S. Sariciftci, S. Bauer, Flexible high power-per-weight perovskite solar cells with chromium oxide-metal contacts for improved stability in air, Nat. Mater. 14 (2015) 1032–1039, https://doi.org/10.1038/nmat4388.
[16] K. Sun, P. Li, Y. Xia, J. Chang, J. Ouyang, Transparent conductive oxide-free perovskite solar cells with PEDOT:PSS as transparent electrode, ACS Appl. Mater. Interfaces 7 (2015) 15314–15320, https://doi.org/10.1021/acsami.5b03171.
[17] H. Lu, J. Sun, H. Zhang, S. Lu, W.C.H. Choy, Room-temperature solution-processed and metal oxide-free nano-composite for the flexible transparent bottom electrode of perovskite solar cells, Nanoscale 8 (2016) 5946–5953, https://doi.org/10.1039/c6nr00011h.
[18] Y. Li, L. Meng, Y. Yang, G. Xu, Z. Hong, Q. Chen, J. You, G. Li, Y. Yang, Y. Li, High-efficiency robust perovskite solar cells on ultrathin flexible substrates, Nat. Commun. 7 (2016) 10214, https://doi.org/10.1038/ncomms10214.
[19] J. Wang, F. Fei, Q. Luo, S. Nie, N. Wu, X. Chen, W. Su, Y. Li, C.Q. Ma, Modification of the highly conductive PEDOT:PSS layer for use in silver nanogrid electrodes for flexible inverted polymer solar cells, ACS Appl. Mater. Interfaces 9 (2017) 7834–7842, https://doi.org/10.1021/acsami.6b16341.
[20] S. Ye, A.R. Rathmell, Z. Chen, I.E. Stewart, B.J. Wiley, Metal nanowire networks: the next generation of transparent conductors, Adv. Mater. 26 (2014) 6670–6687, https://doi.org/10.1002/adma.201402710.
[21] S. Cho, S. Kang, A. Pandya, R. Shanker, Z. Khan, Y. Lee, J. Park, S.L. Craig, H. Ko, Large-area cross-aligned silver nanowire electrodes for flexible, transparent, and force-sensitive mechanochromic touch screens, ACS Nano 11 (2017) 4346–4357, https://doi.org/10.1021/acsnano.7b01714.
[22] E. Lee, J. Ahn, H.C. Kwon, S. Ma, K. Kim, S. Yun, J. Moon, All-solution-processed silver nanowire window electrode-based flexible perovskite solar cells enabled with amorphous metal oxide protection, Adv. Energy Mater. 8 (2018) 11, https://doi.org/10.1002/aenm.201702182.
[23] K. Han, M. Xie, L. Zhang, L. Yan, J. Wei, G. Ji, Q. Luo, J. Lin, Y. Hao, C.Q. Ma, Fully solution processed semi-transparent perovskite solar cells with spray-coated silver nanowires/ZnO composite top electrode, Sol. Energy Mater. Sol. Cells 185 (2018) 399–405, https://doi.org/10.1016/j.solmat.2018.05.048.
[24] M. Xie, J. Wang, J. Kang, L. Zhang, X. Sun, K. Han, Q. Luo, J. Lin, L. Shi, C.-Q. Ma, Super-flexible perovskite solar cells with high power-per-weight on 17 μ m thick PET substrate utilizing printed Ag nanowires bottom and top electrodes, Flex. Print. Electron. 4 (2019), https://doi.org/10.1088/2058-8585/ab2f37, 034002.
[25] M. Xie, H. Lu, L. Zhang, J. Wang, Q. Luo, J. Lin, L. Ba, H. Liu, W. Shen, L. Shi, C. Ma, Fully solution-processed semi-transparent perovskite solar cells with ink-jet printed silver nanowires top electrode, Sol. RRL 2 (2018) 1700184, https://doi.org/10.1002/solr.201700184.

[26] S. Kang, J. Jeong, S. Cho, Y.J. Yoon, S. Park, S. Lim, J.Y. Kim, H. Ko, Ultrathin, lightweight and flexible perovskite solar cells with an excellent power-per-weight performance, J. Mater. Chem. A. 7 (2019) 1107–1114, https://doi.org/10.1039/c8ta10585e.

[27] T.Y. Jin, W. Li, Y.Q. Li, Y.X. Luo, Y. Shen, L.P. Cheng, J.X. Tang, High-performance flexible perovskite solar cells enabled by low-temperature ALD-assisted surface passivation, Adv. Opt. Mater. 6 (2018) 10, https://doi.org/10.1002/adom.201801153.

[28] C.C. Boyd, R. Cheacharoen, K.A. Bush, R. Prasanna, T. Leijtens, M.D. McGehee, Barrier design to prevent metal-induced degradation and improve thermal stability in perovskite solar cells, ACS Energy Lett. 3 (2018) 1772–1778, https://doi.org/10.1021/acsenergylett.8b00926.

[29] J.J. Liang, M. Li, J.Y. Zhu, H. Zong, Y. Zhang, S.M. Jain, Z.K. Wang, Detrimental effect of silver doping in spiro-MeOTAD on the device performance of perovskite solar cells, Org. Electron. 69 (2019) 343–347, https://doi.org/10.1016/j.orgel.2019.03.036.

[30] X. Li, H.H. Ding, G.H. Li, Y. Wang, Z.M. Fang, S.F. Yang, H.X. Ju, J.F. Zhu, In situ investigations of interfacial degradation and ion migration at $CH_3NH_3PbI_3$ perovskite/Ag interfaces, Chin. J. Chem. Phys. 32 (2019) 299–305, https://doi.org/10.1063/1674-0068/cjcp1808189.

[31] A. Kim, Y. Won, K. Woo, S. Jeong, J. Moon, All-solution-processed indium-free transparent composite electrodes based on Ag nanowire and metal oxide for thin-film solar cells, Adv. Funct. Mater. 24 (2014) 2462–2471, https://doi.org/10.1002/adfm.201303518.

[32] S.Y. Ryu, J.H. Seo, H. Hafeez, M. Song, J.Y. Shin, D.H. Kim, Y.C. Jung, C.S. Kim, Effects of the wrinkle structure and flat structure formed during static low-temperature annealing of ZnO on the performance of inverted polymer solar cells, J. Phys. Chem. C 121 (2017) 9191–9201, https://doi.org/10.1021/acs.jpcc.7b02149.

[33] C.F. Lin, C.S. Chen, P.C. Yang, Y.M. Shen, S.Y. Ma, S.C. Shiu, S.C. Hung, S.H. Lin, The influence of wrinkled ZnO on inverted low bandgap thin film solar cells, Sol. Energy Mater. Sol. Cells 101 (2012) 180–185, https://doi.org/10.1016/j.solmat.2012.01.042.

[34] P. Gao, M. Grätzel, M.K. Nazeeruddin, Organohalide lead perovskites for photovoltaic applications, Energy Environ. Sci. 7 (2014) 2448–2463, https://doi.org/10.1039/c4ee00942h.

[35] J. Wang, X. Chen, F. Jiang, Q. Luo, L. Zhang, M. Tan, M. Xie, Y.-Q. Li, Y. Zhou, W. Su, Y. Li, C.-Q. Ma, Electrochemical Corrosion of Ag Electrode in the Silver Grid Electrode-Based Flexible Perovskite Solar Cells and the Suppression Method, vol. 2, 2018, https://doi.org/10.1002/solr.201800118, 1800118.

[36] W. Zhang, M. Saliba, D.T. Moore, S.K. Pathak, M.T. Hörantner, T. Stergiopoulos, S. D. Stranks, G.E. Eperon, J.A. Alexander-Webber, A. Abate, A. Sadhanala, S. Yao, Y. Chen, R.H. Friend, L.A. Estroff, U. Wiesner, H.J. Snaith, Ultrasmooth organic–inorganic perovskite thin-film formation and crystallization for efficient planar heterojunction solar cells, Nat. Commun. 6 (2015) 6142, https://doi.org/10.1038/ncomms7142.

[37] X. Li, S. Fu, S. Liu, Y. Wu, W. Zhang, W. Song, J. Fang, Suppressing the ions-induced degradation for operationally stable perovskite solar cells, Nano Energy 64 (2019) 103962, https://doi.org/10.1016/j.nanoen.2019.103962.

[38] E. Bi, H. Chen, F. Xie, Y. Wu, W. Chen, Y. Su, A. Islam, M. Grätzel, X. Yang, L. Han, Diffusion engineering of ions and charge carriers for stable efficient perovskite solar cells, Nat. Commun. 8 (2017) 15330, https://doi.org/10.1038/ncomms15330.

[39] K. Domanski, B. Roose, T. Matsui, M. Saliba, S.-H. Turren-Cruz, J.-P. Correa-Baena, C.R. Carmona, G. Richardson, J.M. Foster, F. De Angelis, J.M. Ball, A. Petrozza, N. Mine, M.K. Nazeeruddin, W. Tress, M. Grätzel, U. Steiner, A. Hagfeldt, A. Abate, Migration of cations induces reversible performance losses over day/night cycling in perovskite solar cells, Energy Environ. Sci. 10 (2017) 604–613, https://doi.org/10.1039/C6EE03352K.

[40] Y. Kato, L.K. Ono, M. V Lee, S.H. Wang, S.R. Raga, Y.B. Qi, Silver iodide formation in methyl ammonium lead iodide perovskite solar cells with silver top electrodes, Adv. Mater. Interfaces 2 (2015) 6, https://doi.org/10.1002/admi.201500195.

[41] I. Jeon, J. Yoon, N. Ahn, M. Atwa, C. Delacou, A. Anisimov, E.I. Kauppinen, M. Choi, S. Maruyama, Y. Matsuo, Carbon nanotubes versus graphene as flexible transparent electrodes in inverted perovskite solar cells, J. Phys. Chem. Lett. 8 (2017) 5395–5401, https://doi.org/10.1021/acs.jpclett.7b02229.